Enhanced CT/MRI non-rigid brain registration with a custom phantom

Filipa Ferreira Pinto
filipa.f.pinto@tecnico.ulisboa.pt

Instituto Superior Técnico, Universidade de Lisboa, Lisboa, Portugal

December 2020

Abstract

Distortion in magnetic resonance imaging leads to inaccurate location of brain tumours and/or lesions and therefore, MR images need correction in order to overcome that artifact. This correction can be achieved by having as ground truth CT (computed tomography) images and by performing a registration between these two modalities. In this work, many transformations were applied to the raw MR images, and these can be divided into linear and non-linear, depending on the degrees of freedom. Linear registrations were used to firstly align the CT and MR images and the non-linear registrations were then performed to correct the so-called distortion. To achieve the goal of this thesis, two softwares were used: 3D Slicer, to visualization and analysis of medical images and Matlab, a programming platform. A calibration phantom was also necessary, the one chosen consists of a box-shaped grid with equally spaced spheres. This way, one could accurately access the positions of the target CT control points and the MRI deformed points to obtain a transformation capable of bringing these last ones to the desired positions. The best transformation obtained led to a final error with maximum value of 1.55 mm and an average value of 0.64 mm which is below the upper limit necessary to allow for a brain surgery to occur. That transformation was then applied to a real patient MR images to confirm if the correction would work for every object scanned by that specific MRI machine. **Keywords:** Computed Tomography, Magnetic Resonance Imaging, Distortion, Registration, Transformation

1. Introduction

The field of medical imaging has experienced a period of rapid development over the last decades and has consequently revolutionised the way in which modern medicine is practised. The emanation of imaging modalities such as Magnetic Resonance Imaging (MRI), Computed Tomography (CT), Ultrasounds (US) and Positron Emission Tomography (PET), have best owed upon the surgeon and other medical physicians, the ability to peer non-invasively into the human body. This provides the surgeon with not only detailed in vivo information of human anatomy, but also an insight into actual human function. The main aims behind the use of medical imaging however, may be summed up by two objectives: namely diagnosis and therapy. Diagnosis relies on the ability to extract, quantify, and most importantly to interpret all the information obtained from the various imaging modalities. This step is necessary in order to discriminate disease and also to facilitate further therapeutic solutions such as radiotherapy and image guided surgery.

The advent of modern medical image processing techniques arose due to a high demand from clinical applications and this has been one of the underlying motivations behind extensive research into image processing areas [1].

2. Background

MRI, with its ability to distinguish gray matter from white matter - excellent soft tissue contrast - and high SNR (signal to noise ratio), is the diagnostic imaging of choice in the brain. However, despite all the advantages it is subject to geometric image distortions that may seriously decrease the accuracy of a surgery [2, 3, 4]. Reggarding CT, it allows to distinguish the surface of the brain, the ventricles, tumors and at four times the resolution of most MRIs and images can be made much more quickly. Nonetheless, accurate segmentation of the target structures and tumors based on CT alone is challenging due to insufficient image contrast. To compensate for the drawbacks of both image modalities, MRI is used in conjuction with CT for target and tumor delineation, meaning that an accurate registration - procedure of finding a spatial deformation to match two images [5] - between these two is crucial [2, 3]. A registration algorithm can be decomposed into three components: similarity mea-

sure, transformation model and optimization process [6].

2.1. Similarity measure

Registration based on patient image content can be divided into geometric approaches and intensity approaches. Geometric or feature-based methods build explicit models of identifiable anatomical elements in each image. These elements typically include functionally important surfaces, curves and point landmarks that can be matched with their counterparts in the second image. These correspondences define the transformation from one image to the other [6]. Registration using intensity or voxel similarity measures involves calculating the registration transformation by optimizing some measure calculated directly from the voxel values (or pixel values) in the images rather than from geometrical structures [7].

2.2. Transformation model

The transformation model defines how one image (the source image) can be changed to match another (the target image) and it characterizes the type and number of possible deformations [6].

Global linear or rigid transformations are by far the most utilised registration techniques seen throughout the literature and in clinical applications [1] and are characterised by allowing 6 degrees of freedom (DOF): 3 translations and 3 rotations.

The key characteristic of a rigid body transformation is that all distances are preserved [7] - the distance between any two points in an image remains unchanged [1]. Some registration algorithms increase the number of degrees of freedom by allowing for anisotropic scaling, giving 9 DOF. Others, do it so by a transformation that includes scaling and skews as well as the rigid body parameters. These are referred to as affine transformations (12 DOF), and have the important characteristic that all parallel lines are preserved. Projective transformations (15 DOF and rarely used in literature [1]) do not preserve parallelism, length or angles [8]. Affine and projective transformations are both representative of linear transformations and the mathematical expressions of affine transformation can be described in the following matrix form:

$$T_{affine} = \begin{bmatrix} \theta_{11} & \theta_{12} & \theta_{13} \\ \theta_{21} & \theta_{22} & \theta_{23} \\ \theta_{31} & \theta_{32} & \theta_{33} \end{bmatrix} \begin{bmatrix} x \\ y \\ z \end{bmatrix} + \begin{bmatrix} \theta_{14} \\ \theta_{24} \\ \theta_{34} \end{bmatrix}$$

A non-linear or non-rigid registration defines a deformable body where a deformation field gives a translation or mapping for every pixel in the image (multiple DOF).

2.3. Optimization process

The optimization process refers to the manner in which the transformation is adjusted to improve the image similarity and a good optimizer is one that reliably and quickly finds the best possible transformation [1]. Many registration algorithms are amenable to existing optimization schemes in that they seek to choose a set of parameters to maximize (or minimize) a function. Which optimization scheme is suitable for a particular registration application depends on the cost function, the transformation, potential time-constraints, and the required accuracy of the registration [6].

2.4. Validation

Validation of registration results is a very hard matter as the algorithms employed are usually tailored for specific applications. It is also extremely hard to quantitatively measure the accuracy of any particular registration algorithm. Some approaches that have been used to characterise registration accuracy involve the use of 'phantoms'or imaging phantom which is a highly specialized object utilized in medical imaging for quality control, equipment calibration, dosimetry and education [1, 9]. Phantom studies are based on the registration of images that are acquired from either the imaging of a physical phantom, such as a synthetic brain model, or from a software based phantom, i.e. simulated images. Although certain phantom studies are helpful in providing some 'ground truth' information that can be controlled in certain aspects, they are still limited due to the amount of confidence that can be instilled in the results obtained from their use with respect to clinical practice. The accuracy of registration algorithms can be measured both qualitatively and quantitatively. A qualitative approach is generally based on visual inspection by trained medical physicians to see if corresponding structures are effectively overlapped onto each other. A quantitative approach however, relies on more mathematical or statistical techniques in order to quantitatively measure the accuracy [1].

3. Implementation

In this work, a 3D phantom was used to quantify and rectify the MRI distortion. Below one can find an image of the nonanthropomorphic phantom (not based on the human skull) used, named *Matrix* designed in *SolidWorks* [10] and then 3D printed, which consists of a box-shaped grid, made of PLA (Polylactic Acid), with equal spacing spheres with a diameter of 4 mm - reference structures - positioned along the three directions in order to create a 3D array of points. In this particular phantom, the array contains a total of 441 ($9 \times 7 \times 7$) control points spanning an effective volume of $10 \times 8 \times 8$ cm^3 (with intervals of 1 cm along each direction).

Thus, the spatial variation of the geometric distortion can be easily measured with desirable details [11].

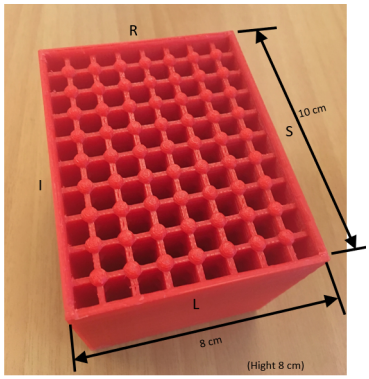

Figure 1: Box-shaped grid phantom - *Matrix*

The geometric distortion within the effective volume of the phantom can be fully described by positional deviations along the three orthogonal axes:

$$dx(r) = x'(r) - x$$
$$dy(r) = y'(r) - y$$
$$dz(r) = z'(r) - z$$
$$\text{or}$$
$$dr(r) = r'(r) - r$$

where x, y and z denote the positions of the control points defined by the geometry of the phantom and x', y' and z' define the positions of the distorted image space. The key parameters used in this scheme include the maximum absolute positional deviations along the x, y and z axes ($|dx|_{max}$, $|dy|_{max}$ and $|dz|_{max}$) and the maximum absolute deviation in the positional vector ($||dr||_{max}$) within a given volume of interest [12].

The phantom was scanned by CT (performed with the Phillips Brilliance R 64) and MRI (using a Phillips 3 Tesla Achieva R in the sagittal plane) as it can be seen in Figure 2 and 3 [13]. It is noticeable the differences between the two image modalities, while in CT the phantom's grid shows up in white and the hydrogel (inserted in the phantom before the scan) in black, for the MRI the opposite happens.

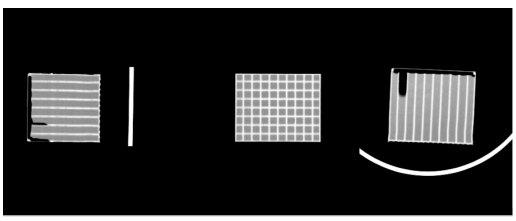

Figure 2: CT of the phantom: sagittal view (left), coronal view (center) and axial view (right).

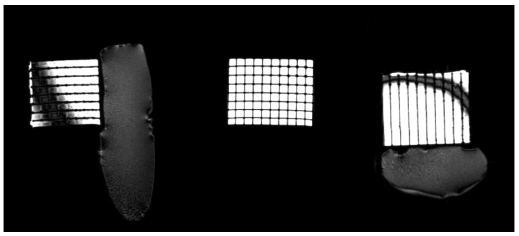

Figure 3: MRI of the phantom: sagittal view (left), coronal view (center) and axial view (right).

3.1. Softwares

In this work two softwares were used: *3D Slicer*, a software application for visualization and analysis of medical image computing data sets [14]; and *Matlab 2020*, a programming platform designed specifically for engineers and scientists [15].

In *3D Slicer*, CT and MR images of the phantom were uploaded which allowed the visualization of its images (2D) and volume (3D) (by using the module *Volume Rendering*). Before starting the registration it is important to notice that the images of both image modalities were centered, to obtain the same origin, and so the same referential, as visible in Figure 4.

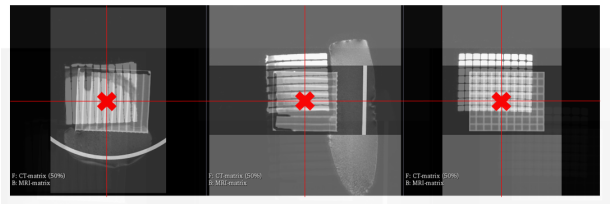

Figure 4: Image Origin.

By using the module *Volume*, the following DICOM (digital imaging and communications in medicine) format informations were given: phantom's CT has an imaging array size of 512 × 512 × 72 and a field of view (FOV), area of anatomy included in an image [16], of 256 mm × 256 mm × 90 mm since the corresponding voxel dimensions were 0.5 mm × 0.5 mm × 1.25 *mm*. Concerning the MRI, it has an image dimension of 512 × 512 × 155, a FOV of 250 mm × 250 mm × 155 mm since voxel dimensions in this case are 0.49 mm × 0.49 mm × 1 mm .

Since for a comprehensive and accurate three-dimensional mapping of the geometric distortion, the two key requirements are a dense distribution of the control points (441 in this case) and a robust and accurate method for the positional measurement of these control points [17] an algorithm was implemented on *Matlab* for that same purpose. It resorts to a detector to find out the locations of the spheres in the given volumes but, since the spheres of the phantom are small, they can be viewed as cor-

ners which mean that a corner detector is needed, in this case, the one chosen was the Harris corner detector.

With the use of both softwares, a symbiosis could be achieved for better understanding of the results. By bringing the spheres of the phantom, segmented by hand and by analysing all the three views of the phantom, to *Matlab*, the initial distances between the target CT points and the distorted MRI were obtained.

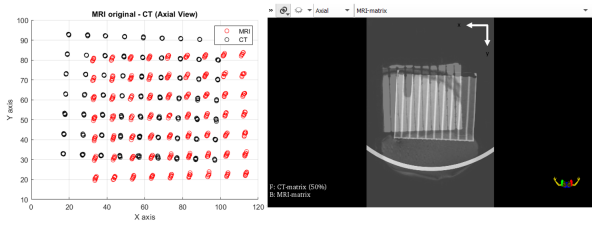

Figure 5: Segmentation in Matlab (left) vs Image on 3D Slicer (right): axial view.

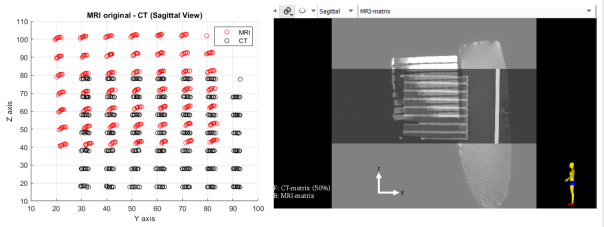

Figure 6: Segmentation in Matlab (left) vs Image on 3D Slicer (right): sagittal view.

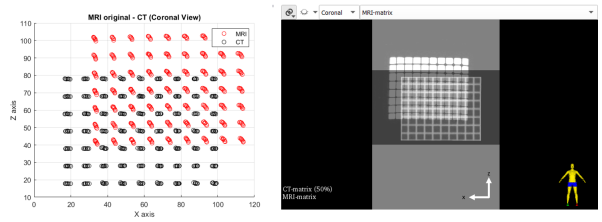

Figure 7: Segmentation in Matlab (left) vs Image on 3D Slicer (right): coronal view.

4. Results

Non-affine registration algorithms normally either include an initial rigid body or affine transformation, or are run after a rigid-body or affine algorithm has provided a starting estimate [7].

BRAINSfit registration module is a module available on *3D Slicer* that registers a three-dimensional volume to a reference volume, by using Mattes Mutual Information (by default) [18]. It offers also other image similarity measures such as Normal Correlation (NC) and Mean Square Error (MSE) which perform better for mono-modal images. The similarity measure in this work will always be the Mattes Mutual Information, based on Mattes et al: CT-PET Registration algorithm [19].

4.1. Rigid Registration

In 3D Slicer, a linear transformation was applied to the MR image in order to obtain an initial raw alignment (qualitative alignment by hand) between the two image modalities by using the module Transforms. This module allows translation and rotation of images - 6 DOF - leading to the following transformation matrix:

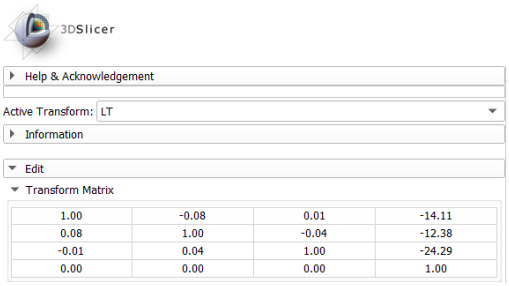

Figure 8: Transformation matrix obtained with module *Transforms*

The results obtained in *3D Slicer* were brought to *Matlab* leading to the following plot showing the spheres centers of the target CT and MRI aligned by hand:

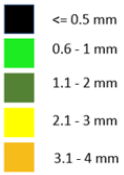

Figure 9: Color bar legend.

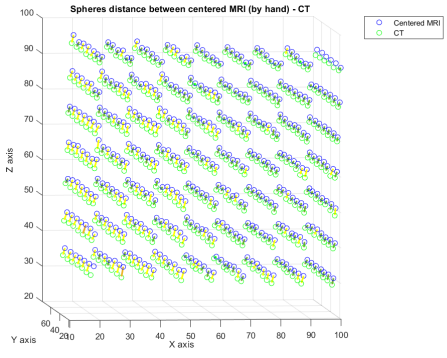

Figure 10: Remaining error in the MRI centered by hand - 1st linear transform.

From the above plot it is possible to infer that there are no distances above 4.1 mm.

To better understand the translations that the spheres performed regarding each axis, another analysis was made, not considering only the magnitude of the distance vector but instead, its components in each direction.

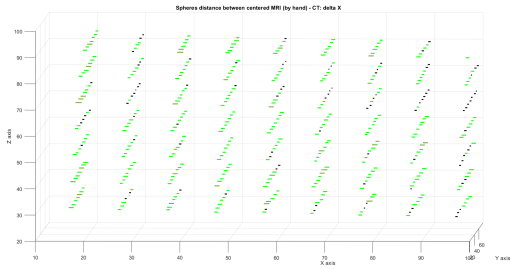

Figure 11: Spheres distance between the centered MRI (by hand) and the target CT in the X-axis.

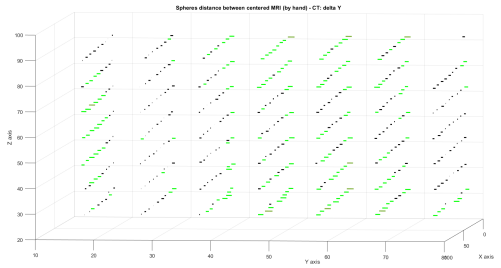

Figure 12: Spheres distance between the centered MRI (by hand) and the target CT in the Y-axis.

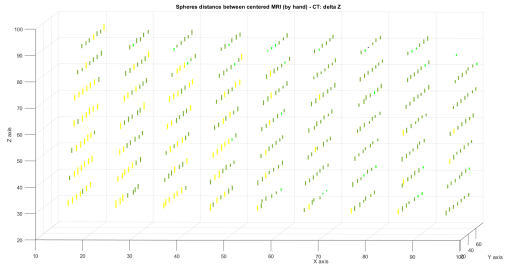

Figure 13: Spheres distance between the centered MRI (by hand) and the target CT in the Z-axis.

The above plots show that the greater distance errors are present in the Z direction and the one which has less influence in the magnitude of the distance vector is the Y direction.

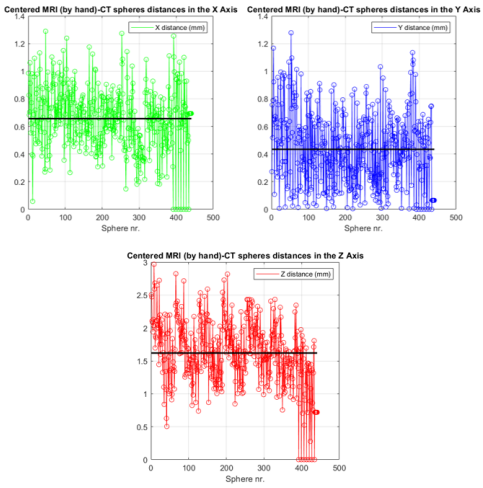

Figure 14: Spheres distance between the centered MRI (by hand) and the target CT in the 3 axis.

Concluding, the average distance value in X is 0.6565 mm, in Y is 0.4346 mm and in Z is 1.6197 mm.

Then, *BRAINSfit* was used to perform an automatic rigid registration and an improved alignment between the volumes in order to prepare the MRI for the deformable transformation. The transform used in this case is a specific type of linear, namely the affine registration, which allows for translation, rotation, scale and shear - 12 DOF. After choosing the similarity measure (MMI), the transformation model (rigid + affine) and the interpolation method (linear), the automatic registration was performed. Even though the first linear transform was based on the entire volume of the phantom, this second registration will vary depending on the method followed as stated in Figure 15.

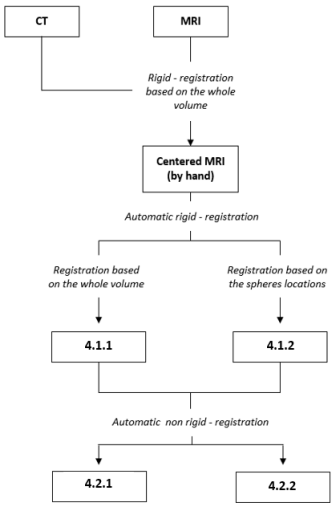

Figure 15: Schematic registration's approaches.

4.1.1 Registration based on the entire volume of the phantom

By using the phantom's CT as the target image and the MRI aligned by hand as the moving image, the obtained linear transform led to the alignment showed in Figure 16.

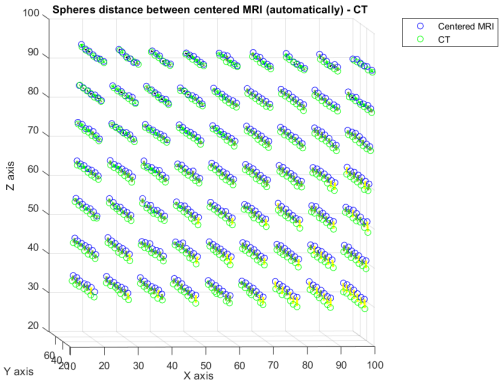

Figure 16: Remaining error in the MRI centered automatically - 2nd linear transform.

The improvement in distance's error between spheres led to a new maximum of 2.95, an average of 1.38 and a minimum of 0.17 mm.

The next step is to analyse the distances between the spheres of aligned MRI and target CT in each axis.

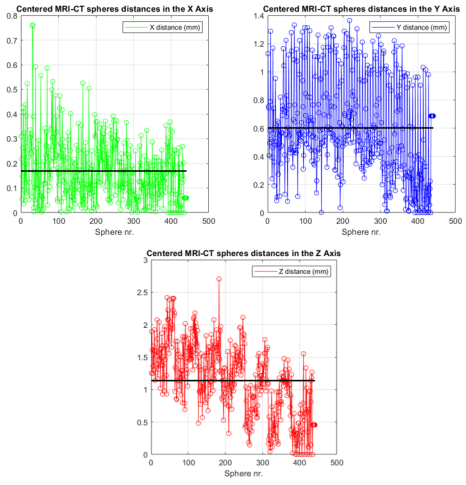

Figure 17: : Spheres distance between the centered MRI and the target CT in the 3 axis.

The above plots show that the distance in the X direction has an average value of 0.1619 mm, the Y direction has an average of 0.6017 mm and the value for Z is 1.1378 mm.

4.1.2 Registration based on the spheres positions

For this registration the target images used were the ones showing, instead of the entire phantom, only the spheres locations in phantom's CT (Figure 18) and the moving images were the ones that showed only the spheres locations of the aligned MRI by hand (Figure 19).

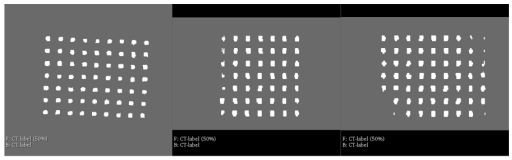

Figure 18: Spheres segmented in phantom's CT.

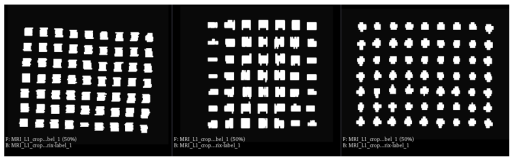

Figure 19: Spheres segmented in phantom's MRI.

The linear transform obtained from 3D Slicer was then applied to the aligned MRI by hand leading to the improved alignment shown below.

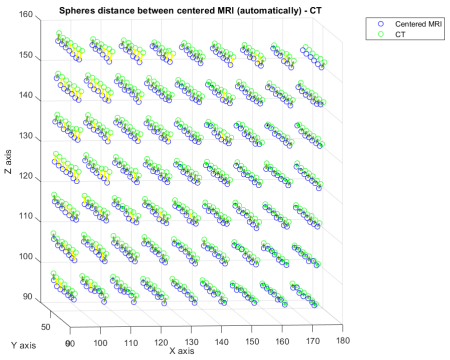

Figure 20: Remaining error in the MRI centered automatically - 2nd linear transform.

The minimum, maximum and average value of distortion in the automatically centered MRI were 0.48, 2.86 and 1.53 mm respectively. Finally, we analyse the distances between MRI-CT spheres in each direction.

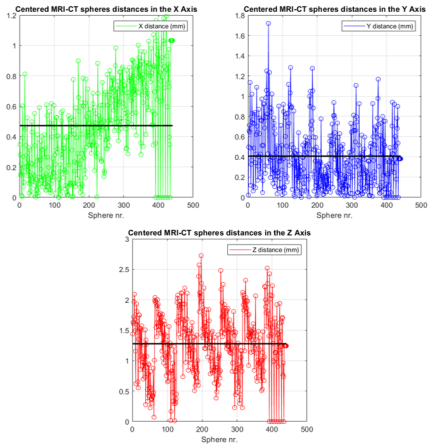

Figure 21: Remaining error in the MRI centered automatically - 2nd linear transform.

In the X direction, the average distance is now 0.4725 mm. In the Y direction it is of 0.4076 mm and in the Z direction, the average is 1.2776 mm.

4.2. Non-rigid registration

A non-rigid registration was then performed by using, once again, BRAINSfit. The only difference was that the transformation model chosen was a deformable one based on B-Splines (> 27 DOF). This deformation model is widely used in image registration due to its good smoothness constraints and because it maintains the shape of the topological invariant and continuous characteristics [20].

4.2.1 Registration based on the entire volume of the phantom

For this step the target image is still the phantom's CT and the moving image is now the MRI aligned automatically using the entire volume.

The results were analysed in *Matlab* and the remaining distortion presented in spheres locations is the following:

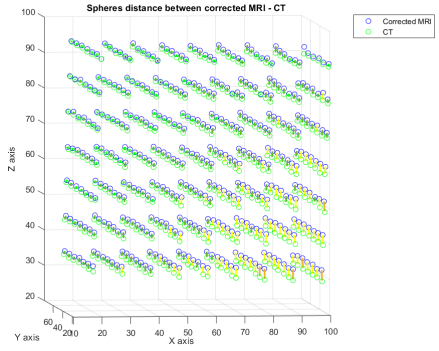

Figure 22: Result for the corrected MR images.

The maximum value was of 3.19, the minimum was 0.47 and the average value was 1.53 mm and the deformation imposed by the B-Spline applied in this case is expressed in Figure 23.

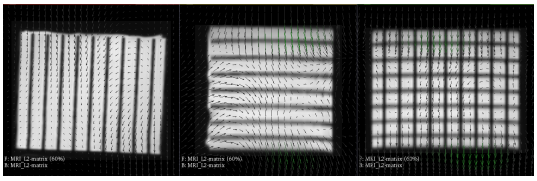

Figure 23: Deformation imposed by the B-Spline.

The next step is to analyse the distances between the spheres of the corrected MRI and target CT in each axis.

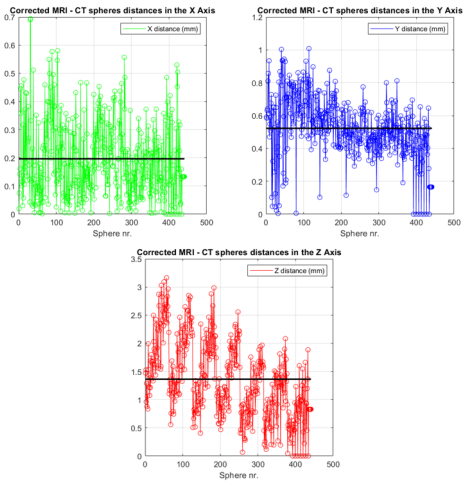

Figure 24: Spheres distance between the corrected MRI and the target CT in the 3 axis.

The above plots show that the distance in the X direction has an average value of 0.1964 mm, the Y direction has an average of 0.5225 mm and the value for Z is 1.3637 mm.

4.2.2 Registration based on the phantom's spheres

The B-Spline transform based on the spheres alone, is supposed to lead to very small remaining errors. The deformable transformation was then applied to the MRI aligned automatically by using the transform obtained by the registration of the images containing the spheres positions. Accuracy was assessed by estimating the measured residual geometric distortions in the corrected images. If the positions of the points have been measured accurately, the corrected images can then be expected to contain little or no geometric distortion [17].

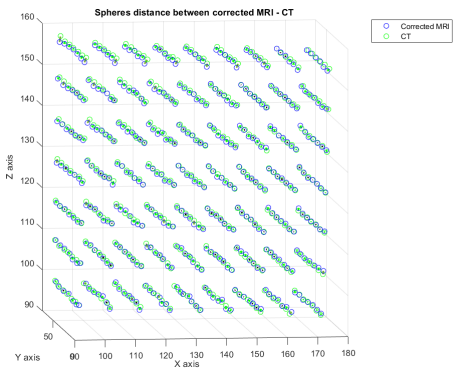

Figure 25: Result for the corrected MR images.

Once again, by analyzing the color scale, it is possible to infer that there are no distortions above 2 mm (no yellow vectors are shown).

The minimum, maximum and average value of the remaining distortion in the non-linearly deformed MRI were 0.08, 1.55 and 0.64 mm respectively and the deformation imposed by the B-Spline applied in this case is expressed in Figure 26.

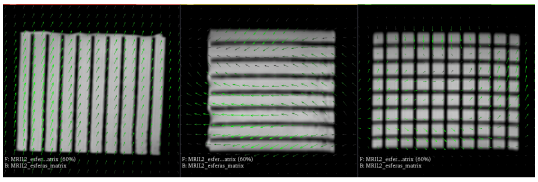

Figure 26: Deformation imposed by the B-Spline.

Finally, the remaining error in the position of the spheres of the corrected MRI in each direction is the following:

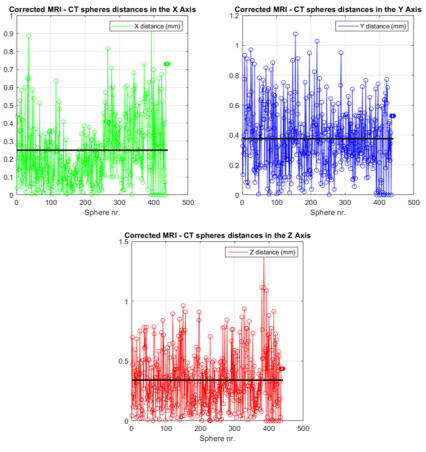

Figure 27: Spheres distance between the corrected MRI and the target CT in the 3 axis.

The average values for the errors in each direction were of 0.2487, 0.3753 and 0.3402 mm for X, Y and Z.

4.3. Discussion of results

As seen in the previous sections, the registration based on phantom's spheres showed better results for the minimum, maximum and average errors for the overall correction; and so it is the most accurate approach.

	Maximum value (mm)	Minimum value (mm)	Average Value (mm)
Volume	3.19	0.47	1.53
Spheres	1.55	0.08	0.64

Table 1: Table of results for the absolute distances between spheres.

	Average X value (mm)	Average Y value (mm)	Average Z value (mm)
Volume	0.1964	0.5225	1.3637
Spheres	0.2487	0.3753	0.3402

Table 2: Table of results for the distances between spheres in each direction.

4.4. Real Patient Results

After obtaining the B-spline transformation, for the grid box-shaped phantom, the next step was to apply it to a real life patient MRI. At the same time, a registration based on the patient's CT and MRI using rigid and non-rigid transformations was also done. In this way it was possible to acquire which method performed a more accurate correction of the distortion, i.e. computed the most suitable B-spline transformation, for the images: 1) the application of a non-linear transform based on a calibration phantom or 2) by using a non-linear transform immediately computed from the patient's images as explained in Figure 28.

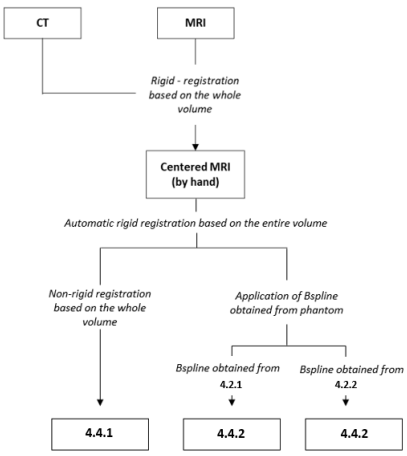

Figure 28: Scheme of registration procedures.

The process of alignment is always the first step towards distortion correction and it was performed in the same as the one described in section 4.1. Therefore, it began with an initial raw alignment with the use of *Transforms* module.

Transform Matrix

1.00	-0.01	-0.00	0.30
0.01	1.00	-0.00	1.04
-0.01	0.00	0.99	-3.86
0.00	0.00	0.00	1.00

Figure 29: Transformation Matrix.

The second step was also to find a linear transform, but in this case, using an automatic algorithm by using BRAINSfit. This step is to make sure that the images are well aligned and ready to suffer a deformable transformation. As said before the last step of the registration of both images is the only one that differs.

4.4.1 Direct Registration

In this first case, one used once again BRAINSfit to perform the automatic non-rigid registration based on B-Splines. Here, the target image was the patient's CT and the moving image was its aligned MRI.

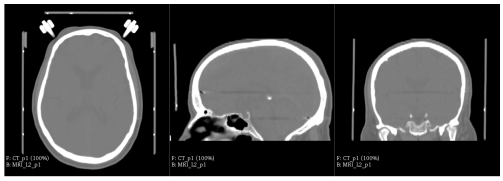

Figure 30: Patient's CT - Target Image.

Figure 31: Patient's Aligned MRI - Moving Image.

4.4.2 Application of the B-Spline from calibration

It is important to notice that the phantom is much smaller than the volume of a human head, therefore, the B-Spline previously calculated using the phantom can only be applied in the volume of the brain that coincides with its location (see Figure 32). Furthermore, the B-Spline transform can only be applied when the CT and MR images of the patient are already aligned, by hand and automatically. It is important to mention that an assumption was made based on the believe that the MR images from the phantom and from the patient were aligned at the time of the acquisition so that the magnetic field could be the same for the same voxel positions in both volumes. Only with this assumption being real is the correction going to work for the patient's MRIs.

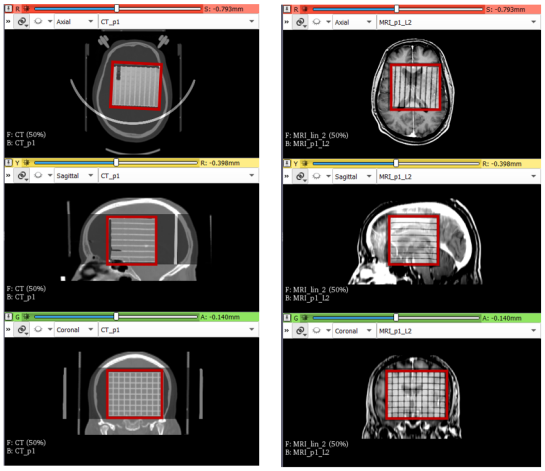

Figure 32: Delimitation of the area where the B-Spline transform can be applied.

4.4.3 Comparison

The next step is to compare the MR corrected images to the target CT in order to evaluate the TRE, even if in a grotesque way. The points chosen in the images were plotted on *Matlab* and their errors can be found below, firstly for the saggital view and lastly for the coronal view.

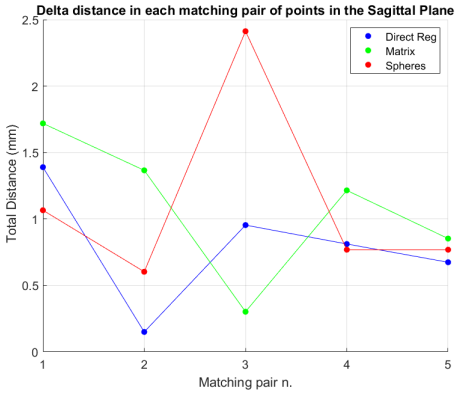

Figure 33: Overall TRE for the different approaches - Sagittal Plane

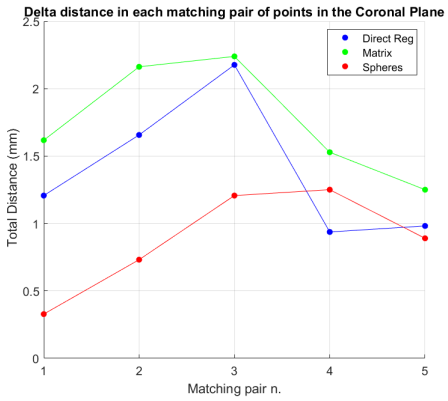

Figure 34: Overall TRE for the different approaches - Coronal Plane

From the above plots, one can conclude that the correction based on the spheres of the phantom obtained the smallest error for a total of 6 chosen points (4 in the coronal view and 2 in the sagittal plane). The correction based on the direct registration of the patient acquired the best results for 3 points (1 in the coronal view and 2 in the sagittal plane). The last approach, which was the one based on the registration of the entire phantom got the best result only once, and for the sagittal plane. Moreover, by summing up the values obtained for the sagittal and coronal views, the total values obtained were the following:

	Sum of Average TREs (mm)
Matrix	2.8509
Spheres	2.0053
Direct Registration	2.1879

Table 3: Sum of average results for the TRE.

given an overall best result for the spheres-based registration and the worst result for the phantom-based one. Concluding, the values obtained for the TRE assign the best distortion correction to the registration based on the spheres of the phantom.

5. Conclusions

This work focused on correcting the distortion inherent in a T1 contrast MRI based on the information contained in the corresponding CT images. This correction will allow the MRI scans to produce images with smaller errors in order to accurately locate brain tumours and/or lesions. In order to achieve this correction one started by working with a box-grid shaped phantom for calibration to precisely compute the errors in the MR images, having as target the corresponding CT images, and eliminate them by registration. The first step was to roughly align the images of the two modalities in order to increase the accuracy for the following automatic registration procedures, starting by a rigid registration followed by a non-rigid one. Two approaches were followed to verify which one would give better results; the first one is a registration based on the entire phantom and the second one is solely based on the spheres positions of the same phantom. The overall results showed that the second method performed better than the first one. After the non-rigid transformations were obtained by both approaches, they were used in a real patient images with the addition of a third method based on the direct registration of the CT and MR images of the patient. Features were then selected in the corrected images and in the target CT to compute the target registration error (TRE). The calculation of the final error was necessary to conclude that, in fact, the registration based on the spheres of the phantom was the best correction and that the worse was the one based on the registration of the entire phantom.

For future work, the creation of a new phantom with the size and shape of a human head with a grid of hundreds of points (more than 441) could be of interest since the distribution of the distortion will be similar to the one present in the images of the head of a real patient. A phantom with the characteristics mentioned before has already been developed by CIRS (Computerized Imaging Reference Systems, Inc.) [21] at the same time this work was being developed and a study based on the distortion captured by that specific phantom can also be visualized in [22, 23, 24] and used for further understanding of the matter. Moreover, in the case of this project, the phantom's volume could not cover the entire volume of a human head and so the correction obtained only works for the volume of the head coincident with the volume of the phantom.

Acknowledgements

I would like to express my gratitude to Professor Jorge Martins for the guidance throughout this journey and to Dr. Herculano, thank you for all the wise inputs and feedbacks.

References

[1] C. Fookes and M. Bennamou, "Rigid and non-rigid image registration and its association with mutual information: A review," tech. rep., Research Concentration in Computer Vision and Automation, School of Electrical and Electronic Systems Engineering, Queensland University of Technology, G.P.O. Box 2434, Qld, 4001, Australia, May 2002.

[2] A. J. Golby, ed., *Image Guided Neurosurgery*. OKYO Academic Press, Elsevier, 2015.

[3] S. Roy, A. Carass, A. Jog, J. L. Prince, and J. Lee, "Mr to ct registration of brains using image synthesis," *Proceedings of SPIE - The International Society for Optical Engineering*, Mar. 2014.

[4] M. Breeuwer, W. Zylka, J. Wadley, and A. Falk, "Detection and correction of geometric distortion in 3d ct/mr images," *Proceedings of SPIE - The International Society for Optical Engineering*, Feb. 2001.

[5] Z. Wu, T. Lan, J. Wang, Y. Ding, and Z. Qin, *Medical Image Registration Using B-Spline Transform*. School of Information and Software Engineering, University of Electronic Science and Technology of China, Jan. 2016.

[6] W. R. Crum, T. Hartkens, and D. L. G. Hill, "Non-rigid image registration: theory and practice," *The British Journal of Radiology*, Feb. 2004.

[7] D. Hill, P. Batchelor, M. Holden, and D. Hawkes, "Medical image registration," *Physics in medicine and biology*, 2000.

[8] G. Mill, "Affine and projective transformations." https://www.graphicsmill.com/docs/gm/affine-and-projective-transformations.htm.

[9] D. J. Bell and C. Hacking, "Phantom." https://radiopaedia.org/articles/phantom.

[10] D. S. S. Corporation, "Solidworks." https://www.solidworks.com/.

[11] C. W. Condo, "Image processing and registration to quantify and rectify mri distortion," Master's thesis, Instituto Superior Técnico, 2017.

[12] D. Wang and D. M. Doddrell, "Geometric distortion in structural magnetic resonance imaging," in *Current Medical Imaging Reviews*, vol. 1, pp. 49–60, Centre for Magnetic Resonance, The University of Queensland, St. Lucia, QLD 4072, Australia: Bentham Science Publishers Ltd., 2005.

[13] P. D. Batista, I. P. Machado, P. Roios, J. Lavrador, M. B. Cattoni, J. Martins, and H. Carvalho, "Position and orientation errors in a neuronavigation procedure: A stepwise protocol using a cranial phantom," *World Neurosurgery*, vol. 126, pp. e342 – e350, 2019.

[14] A. Fedorov, R. Beichel, J. Kalpathy-Cramer, J. Finet, J.-C. Fillion-Robin, S. Pujol, C. Bauer, D. Jennings, F. Fennessy, M. Sonka, J. Buatti, S. Aylward, J. V. Miller, S. Pieper, and R. Kikinis, "3d slicer as an image computing platform for the quantitative imaging network.." https://slicer.readthedocs.io/en/latest/user_guide/about.html.

[15] MathWorks, "What is matlab?." https://www.mathworks.com/discovery/what-is-matlab.html.

[16] M. D. for the Health Professions and F. Nursing, "Field of view." https://medical-dictionary.thefreedictionary.com/field+of+view.

[17] D. Wang, D. M. Doddrell, and G. Cowin, "A novel phantom and method for comprehensive 3-dimensional measurement and correction of geometric distortion in magnetic resonance imaging," *Magnetic Resonance Imaging*, vol. 22, pp. 529–542, Jan. 2004.

[18] H. Johnson, "Documentation/4.4/modules/brainsfit." https://www.slicer.org/wiki/Documentation/4.4/Modules/BRAINSFit.

[19] D. Mattes, D. R. Haynor, H. Vesselle, T. K. Lewellen, and W. Eubank, "Pet-ct image registration in the chest using free-form deformations," *IEEE Transactions On Medical Imaging*, vol. 22, Jan. 2003.

[20] M. Wang and P. Li, "A review of deformation models in medical image registration," *Journal of Medical and Biological Engineering*, 2018.

[21] I. Computerized Imaging Reference Systems, "Mr distortion & image fusion head phantom." https://www.cirsinc.com/products/radiation-therapy/mr-distortion-image-fusion-head-phantom/.

[22] C. Greenwald, M. Lazea, and N. Venugopal, "Pre-clinical validation of open source tools to calculate and track mr distortion using both small and large field of view phantoms," tech. rep., University of Saskatchewan, 2018.

[23] J. Peerlingsa, I. Comptera, F. Janssena, C. J. Wigginsc, A. A. Postmab, F. M. Mottaghyb, P. Lambina, and A. L. Hoffmann, "Characterizing geometrical accuracy in clinically optimised 7t and 3t magnetic resonance images for high-precision radiation treatment of brain tumours.," *Elsevier*, 2019.

[24] P. World, "Getting to grips with mr image distortion." physicsworld.com/a/getting-to-grips-with-mr-image-distortion/.